Chemical Science

ROYAL SOCIETY OF CHEMISTRY

EDGE ARTICLE

View Article Online
View Journal | View Issue

Cite this: *Chem. Sci.*, 2022, **13**, 4372

All publication charges for this article have been paid for by the Royal Society of Chemistry

Received 7th January 2022
Accepted 21st March 2022

DOI: 10.1039/d2sc00111j

rsc.li/chemical-science

Amplification of weak chiral inductions for excellent control over the helical orientation of discrete topologically chiral $(M_3L_2)_n$ polyhedra†

Yuya Domoto, *[a] Kidai Yamamoto,[a] Shumpei Horie,[a] Zhengsu Yu[a] and Makoto Fujita*[ab]

Superb control over the helical chirality of discrete $(M_3L_2)_n$ polyhedra (n = 2,4,8, M = Cu^I or Ag^I) created from the self-assembly of propeller-shaped ligands (L) equipped with chiral side chains is demonstrated here. Almost perfect chiral induction (>99 : 1) of the helical orientation of the framework was achieved for the largest $(M_3L_2)_8$ cube with 48 small chiral side chains (diameter: ~5 nm), while no or moderate chiral induction was observed for smaller polyhedra (n = 2, 4). Thus, amplification of the weak chiral inductions of each ligand unit is an efficient way to control the chirality of large discrete nanostructures with high structural complexity.

Introduction

Amplification of chiral induction has previously been observed in double asymmetric synthesis,[1] where high enantioselectivity or diastereoselectivity arises from two or more chiral sources (*e.g.*, a chiral substrate and a chiral reagent). With increasing multiplication number (m), the selectivity should be exponentially enhanced because the small free energy differences (ΔE_m) that arise from each chiral source accumulate. This process roughly follows the Gibbs free energy equation, $\Delta G = \Sigma \Delta E_m = -RT \ln K$, where K is the reaction selectivity or the equilibrium constant of the two states. Exceptional amplification effects have often been observed in polymeric systems, particularly in the formation of helices in long-chain polymers, where the helical sense of the polymer main chain can be perfectly controlled, even when the chiral induction at every monomer unit is small.[2–4] In discrete molecular systems, however, there are only a limited number of examples where large amplification effects have been observed,[5,6] given that the incorporation of a large number of chiral sources into discrete molecular structures is usually not straightforward. In particular, chirality control over huge and complex discrete nanoarchitectures is believed to open up new concepts in the fields of material science including artificial reaction systems, sensors, and biochemical applications in higher degree of multicomponent manners.[7]

We have recently reported a number of $(M_3L_2)_n$ polyhedra (**2a–4a**; n = 2, 4, 8; M = Cu^I or Ag^I; Fig. 1)[8] constructed from ligand **1a** through conventional metal–pyridyl coordination[9] and secondary metal–acetylene π-coordination.[10] The propeller-shaped tripodal ligand **1a** can exist in two enantiomeric conformations (Fig. 1a) and, once coordinated to M, oligomerizes to form polyhedral frameworks with diameters of up to *ca.* 5 nm (Fig. 1b). Crystallographic and spectroscopic studies have shown that the helical sense of all the **1a** ligands in the polyhedral frameworks are identical, although the polyhedra exist as racemates. We observed that the $(M_3L_2)_n$ polyhedra have many identical ligand arms directed to outer environments, and thus, substantial chiral induction in the polyhedral frameworks retaining cavity structures could be expected by simply introducing a chiral element to the ligand arm. In addition, note that a series of the $(M_3L_2)_n$ polyhedra contain highly entangled structures based on trifurcate motifs,[11–13] exceeding the well classified topologies of conventional knots and links.[14] As these structures are inherently topologically chiral,[15] it is expected to be interesting to demonstrate their precise regulation for invoking future applications of the newly exploited three-dimensional molecular entanglements.

Therefore, in this study, we designed and synthesized ligands **1b–e** (Fig. 1a), which are derivatives of **1a** equipped with a chiral substituent on every arm. We found that, while chiral induction from the side chains is negligible or very small for polyhedra **2** (n = 2) and **3** (n = 4), perfect control over the helicity can be achieved in cubic octamer **4** (n = 8) *via* the remarkable amplification effect of, in total, 48 chiral substituents on the ligand arms. This result demonstrates that the chirality of

[a]*Department of Applied Chemistry, The University of Tokyo, 7-3-1 Hongo, Bunkyo-ku, Tokyo 113-8656, Japan. E-mail: domoto@appchem.t.u-tokyo.ac.jp; mfujita@appchem.t.u-tokyo.ac.jp*

[b]*Division of Advanced Molecular Science, Institute for Molecular Science, National Institutes of Natural Sciences, 5-1 Higashiyama, Myodaiji-cho, Okazaki-shi, Aichi 444-8787, Japan*

† Electronic supplementary information (ESI) available: Synthesis details, spectroscopic characterization, and X-ray crystallography data. CCDC 2108704. For ESI and crystallographic data in CIF or other electronic format see DOI: 10.1039/d2sc00111j

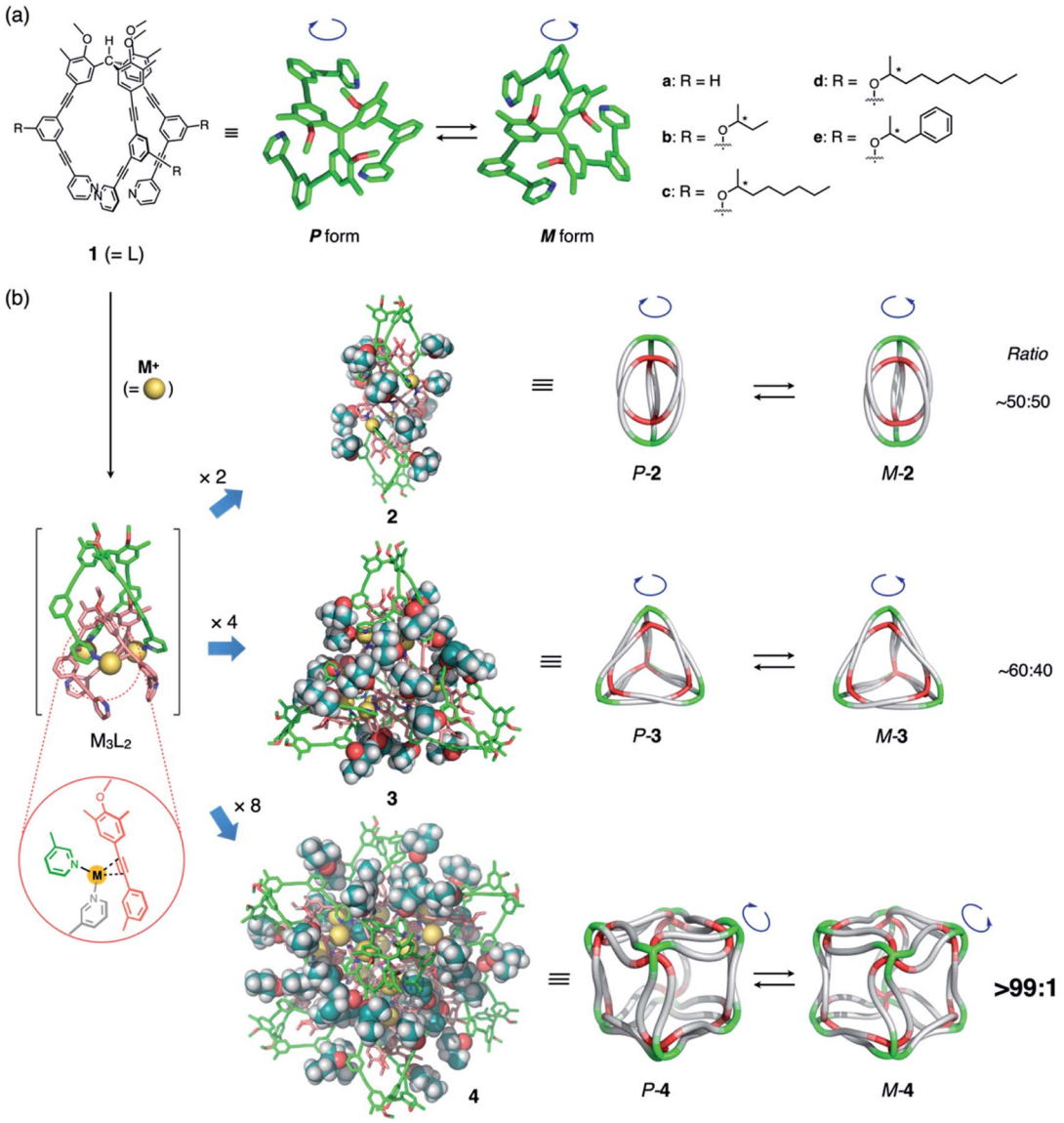

Fig. 1 (a) Chemical structure of propeller-shaped ligand **1** and its *P*- and *M*-forms. Unless otherwise noted, the (*S*)-2-alkoxy isomers of **1b–e** were used in the main study. (b) Schematic representation of the self-assembly of the $(M_3L_2)_n$ coordination polyhedra **2–4** ($n = 2, 4, 8$) with chiral side chains. Each assembly is formed by the oligomerization of n units of M_3L_2, a hypothetical intermediate stabilized by metal–acetylene π-coordination. Illustrations in the second column from the left were generated by combining 2-butoxy side chains (molecular-mechanics (MM) models) with polyhedral frameworks based on the reported crystal structures.[8a,c] Cartoon illustrations in the third column exhibit the entangled structures[11] of the $(M_3L_2)_n$ polyhedra, while metal–acetylene π-coordination is omitted for clarity.[8c]

discrete nanostructures assembled from numerous components can be easily controlled by the amplification effect of weakly chiral elements present on every component.

Results and discussion

Propeller-shaped tripodal ligands **1b–e**, which bear chiral (*S*)-alkoxy side chains on each arm, were designed and prepared according to literature procedures (for details, see the ESI†).[8a,16] Firstly, dimeric $(M_3L_2)_2$ cages **2** were synthesized by mixing $[Cu(MeCN)_4]BF_4$ (1.5 equiv., 3.75 mM) with ligand **1b** in CD_3NO_2. The ^1H NMR spectra showed two sets of proton signals attributable to dimer **2b** (Fig. 2b and S1†), suggesting the formation of two diastereomeric cages with the ligands in either the *M*- or *P*-configuration. However, the diastereomeric ratio was ~1 : 1 in both cases even though a chiral substituent is present on each of the 12 side chains. A lack of chiral induction in the $(M_3L_2)_2$ cage frameworks was also confirmed by the circular dichroism (CD) spectra, which showed no chiral amplification in comparison with the CD spectra of the ligand solutions (Fig. S2†). This absence of chiral induction is presumably due to insufficient steric interactions between the chiral side chains and the cage framework of **2b**. In fact, the single-crystal X-ray structure of the cage framework of **2b** (Fig. 2d) revealed almost no steric crowding between the side chains and the cage framework. We thus examined ligand **1e**

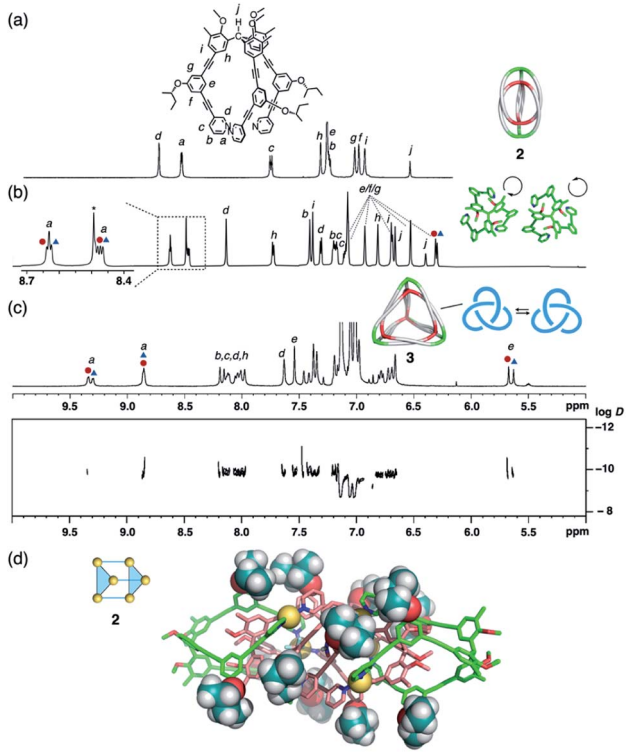

Fig. 2 Self-assembly of complex **2b** and tetrahedron **3b**. Partial ^{1}H NMR spectra of (a) ligand **1b** (500 MHz, 300 K, $CDCl_3$), (b) complex **2b** (700 MHz, 300 K, CD_3NO_2), and (c) tetrahedron **3b** (500 MHz, 300 K, toluene-d_8). Red circles and blue triangles indicate two diastereomeric complexes, respectively. A ^{1}H DOSY spectrum is shown in addition (for details, see Fig. S5†). (d) X-ray crystal structure of **2b**; 2-butoxy chains are shown as space-filling models.

with a sterically more crowded (*S*)-1-phenyl-2-propanoxy group as the chiral substituent (for details, see the ESI†). When cage **2e** was assembled from ligand **1e**, a small amount of diastereoselectivity was observed (62 : 38 by ^{1}H NMR analysis; Fig. S3†), which can be interpreted in terms of increased steric crowding of the bulky groups on the cage (MM model based on partially refined X-ray data; *cf.* Fig. S4†).

The small chiral induction effect observed for cage **2e** encouraged us to examine higher-order oligomeric cages, in which a larger number of chiral side chains are present. The self-assembly of tetrahedral $(M_3L_2)_4$ **3** was thus examined with ligands **1b**. After complexation with $CuBF_4$ (1.5 equiv., 3.75 mM; 50 °C for 30 min) in toluene-d_8, the formation of **3b** was confirmed by ^{1}H and ^{13}C NMR (Fig. 2c and S27–S28†), in addition to ^{1}H diffusion ordered spectroscopy (DOSY) showing a hydrodynamic diameter of ~4.7 nm ($\log D = -9.8$ at 300 K) comparable to that was determined for **3a** by X-ray analysis (4.5 nm).[8a] Here, however, only small diastereomeric ratio (52 : 48) was observed by ^{1}H NMR (Fig. 2c), which is consistent with the moderately enhanced absorption observed in the CD spectra (Fig. S6†).[17]

The helical orientation of ligand **1** forces the generation of a chiral trefoil knot topology[14] on every face of the tetrahedral cage **3** (Fig. 2c, right). In this situation, the two enantiomeric forms cannot be interconverted unless the trefoil knot topology is dissociated. Thus, the *P*- and *M*-helical orientations of the ligand do not interconvert, except under very slow equilibration *via* bond dissociation. Therefore, as shown by variable-temperature (VT) ^{1}H NMR experiments (Fig. S7†), the diastereomeric ratio of **3** is not affected by a change in temperature between 273 and 323 K.[18]

We expected to see a further enhancement in the chiral induction in the $(M_3L_2)_n$ assembly of cube-structured **4** ($n = 8$). As previously reported,[8c] cube **4** can only be constructed *via* the anion-templated conversion of pre-synthesized dimeric cages of **2**. Thus, cage **2d** was prepared by mixing ligand **1d** (with an (*S*)-2-decanoxy side chain, 2.5 mM) and $AgPF_6$ (1.9 equiv.) in $CDCl_3$/CD_3OD (97/3, v/v) at 50 °C for 30 min. Finally, the solution was treated with tetramethylammonium nitrate ($TMANO_3$, 1.0 equiv. in CD_3OD at room temperature over 21 h; $CDCl_3$/CD_3OD ratio after the template addition was 94/6, v/v) (Fig. 3a).[19]

To our surprise, we observed the exclusive formation of only one diastereomer of cube **4d** (>99 : 1) *via* ^{1}H NMR spectroscopy (Fig. 3b and S11a†). Time-dependent NMR measurements

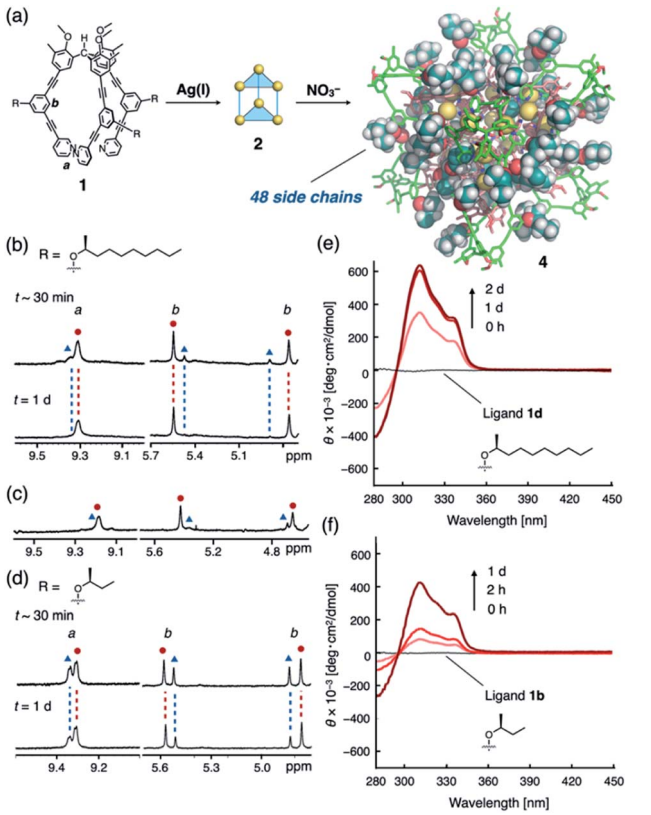

Fig. 3 Self-assembly of cube **4** with ligands that contain chiral side chains. (a) Schematic representation of the nitrate-templated self-assembly of **4** (depicted with R = 2-butoxy for simplicity); partial ^{1}H NMR spectra (500 MHz, 287 K, $CDCl_3$/CD_3OD (94/6, v/v)) of ligand **1d** and cube **4** showing (b) time-dependent redistribution of the diastereomers, (c) cube **4** with ligand **1d** in $CDCl_3$/CD_3OD (97/3, v/v, $t = 18$ h), and (d) cube **4** with ligand **1b** in $CDCl_3$/CD_3OD (97/3, v/v). (e) Changes in the CD (293 K, $CHCl_3$/MeOH (94/6, v/v)) spectrum upon formation of cube **4d**. (f) Changes in the CD (293 K, $CHCl_3$/MeOH (97/3, v/v)) spectrum upon formation of cube **4b**.

revealed that the selectivity is thermodynamically controlled. Immediately following the addition of $TMANO_3$ (~30 min), we observed a relatively low selectivity (82 : 18) that increased to >99 : 1 after stirring the solution for 21 h. This kinetic-to-thermodynamic conversion process was also monitored using CD spectroscopy (Fig. 3e). As precursor **2** is a ~1 : 1 mixture of diastereomers, the relatively rapid interconversion of **2** to **4** by addition of nitrate initially results in the formation of a kinetic mixture of diastereomers of **4d**, which is then converted into the thermodynamic product. Cage **4** was characterized by comparing the ^{1}H and ^{13}C NMR spectra of **4** (Fig. S12†)[20] with those of the previously reported **4a**.[8c] ^{1}H DOSY measurements indicated the formation of a single species with a diffusion coefficient of $D = 1.6 \times 10^{-10}$ m^2 s^{-1} ($\log D = -9.8$ at 287 K; Fig. S13†).

The use of high polarity solvents ($CDCl_3/CD_3OD$ (94/6, v/v)) is particularly important to achieve high selectivity. In fact, when the same experiment was conducted in a slightly less polar solvent ($CDCl_3/CD_3OD$ (97/3, v/v)), the selectivity decreased significantly (max.: 85 : 15; Fig. 3c and S11b†). Presumably, the steric contact of long hydrophobic alkyl chains with the framework of cube **4d** becomes more efficient in polar solvents, thus enhancing the chiral induction, as observed in helical polymers.[4]

To clarify the secondary steric effects, ligands **1c** and **1b** with shorter (*S*)-2-alkoxy side chains were used in the self-assembly of cube **4**. In $CDCl_3/CD_3OD$ (97/3, v/v), a ligand with a 2-octoxy chain (**1c**) offered comparable selectivity (84 : 16; Fig. S15–S16†) to that of **1d** (85 : 15). In the case of **1b**, *i.e.*, a ligand with a much shorter 2-butoxy chain, much lower selectivity (70 : 30) was observed even after 18 h of treatment with tetrabutylammonium nitrate ($TBANO_3$) (Fig. 3d and f).

The *P* and *M* equilibrium constant (*K*) can be described by the Gibbs free energy equation, $K = \exp(-\Delta G/RT)$, where ΔG may roughly be described as $m \cdot E_h$ (E_h: energy difference per chiral unit).[4a,b] Even though E_h is very small, the accumulation of 48 chiral units ($m = 48$) in **4d** is enough to induce a relatively large ΔG that accounts for the perfect chiral induction. In other words, the diastereomeric ratio of 99 : 1 for cube **4** ($n = 8$, $m = 48$) can be ascribed to an energy difference of only -0.23 kJ mol^{-1} per chiral group. Whilst the absolute value is small, the accumulation of 48 chiral groups on the surface of the polyhedron can generate a large ΔG that perfectly controls the chirality of the huge polyhedral framework.

Conclusions

In conclusion, we have successfully controlled the helicity of discrete $(M_3L_2)_n$ polyhedra by adding small chiral side chains to their highly entangled higher-order frameworks. The results shown here are inspiring as they allow the precise structural regulation of large, complex nanoarchitectures, that are usually difficult to synthesize *via* the self-assembly of numerous components. This strategy can be expected to stimulate new approaches toward advanced functional nanomaterials[15] based on discrete molecular designs.‡

Data availability

All the data are shown in the ESI.†

Author contributions

Y. D. and M. F. conceived and designed the study. Y. D. and M. F. co-wrote the paper. Y. D., K. Y., S. H., and Z. Y. performed the chemical experiments and analysed the data. All authors discussed the results and commented on the manuscript.

Conflicts of interest

There are no conflicts to declare.

Acknowledgements

This research was supported by JSPS KAKENHI grants 19H05461 (to M. F.) and 19K05416 (to Y. D.). Y. D. also acknowledges financial support from the Izumi Science and Technology Foundation, Konica Minolta, Inc., and the Society of Synthetic Organic Chemistry (Japan). The authors thank Dr Tadateru Nishikawa (JEOL RESONANCE Inc.) for assistance with the NMR measurements. Synchrotron X-ray crystallography was performed using the BL26B1 beamline at SPring-8 under proposal numbers 2020A0168 and 2021B1246. We thank the Instrument Center at the Institute for Molecular Sciences (Okazaki, Japan) for providing access to CD spectrometers. This work was partly supported by the Nanotechnology Platform Program 'Molecule and Material Synthesis' (JPMXP09S21MS0008) of the Japanese Ministry of Education, Culture, Sports, Science and Technology (MEXT).

Notes and references

‡ Crystallographic data for **2b**: $M = 20583.18$, monoclinic, space group $P2_1/n$, $a = 18.838(4)$ Å, $b = 32.458(6)$ Å, $c = 64.439(13)$ Å, $\alpha = \gamma = 90°$, $\beta = 94.55(3)°$, $V = 39277(14)$ Å^3, $Z = 1$, $D_c = 0.870$ g cm^{-3}, $T = 100(2)$ K, $1.784 < \theta < 47.56°$, 20892 unique reflections out of 69369 with $I > 2\sigma(I)$, GoF = 1.290, final *R* factors $R_1 = 0.1440$ ($I > 2\sigma(I)$), w$R_2 = 0.3746$, CCDC deposition number 2108704.

1 S. Masamune, W. Choy, J. S. Petersen and L. R. Sita, *Angew. Chem., Int. Ed.*, 1985, **24**, 1–30.
2 Y. Okamoto, H. Mohri, T. Nakano and K. Hatada, *J. Am. Chem. Soc.*, 1989, **111**, 5952–5954.
3 (*a*) M. M. Green, C. Andreola, B. Muñoz and M. P. Reidy, *J. Am. Chem. Soc.*, 1988, **110**, 4063–4065; (*b*) M. M. Green, N. C. Peterson, T. Sato, A. Teramoto, R. Cook and S. Lifson, *Science*, 1995, **268**, 1860–1866; (*c*) H. Nakako, R. Nomura and T. Masuda, *Macromolecules*, 2001, **34**, 1496–1502.
4 (*a*) T. Yamada, Y. Nagata and M. Suginome, *Chem. Commun.*, 2010, **46**, 4914–4916; (*b*) Y. Nagata, T. Yamada, T. Adachi, Y. Akai, T. Yamamoto and M. Suginome, *J. Am. Chem. Soc.*, 2013, **135**, 10104–10113; (*c*) Y. Nagata, T. Nishikawa, M. Suginome, S. Sato, M. Sugiyama, L. Porcar, A. Martel, R. Inoue and N. Sato, *J. Am. Chem. Soc.*, 2018, **140**, 2722–2726.
5 (*a*) N. Ousaka, J. K. Clegg and J. R. Nitschke, *Angew. Chem., Int. Ed.*, 2012, **51**, 1464–1468; (*b*) F. Huang, L. Ma, Y. Che,

H. Jiang, X. Chen and Y. Wang, *J. Org. Chem.*, 2018, **83**, 733–739; (*c*) J. Zhang, D. Luo, C. Ma, L. Huang and Q. Gan, *Nat. Commun.*, 2021, **12**, 2659.

6 (*a*) K. S. Jeong, Y. S. Kim, Y. J. Kim, E. Lee, J. H. Yoon, W. H. Park, Y. W. Park, S.-J. Jeon, Z. H. Kim, J. Kim and N. Jeong, *Angew. Chem., Int. Ed.*, 2006, **45**, 8134–8138; (*b*) C. Gütz, R. Hovorka, C. Klein, Q.-Q. Jiang, C. Bannwarth, M. Engeser, C. Schmuck, W. Assenmacher, W. Mader, F. Topić, K. Rissanen, S. Grimme and A. Lützen, *Angew. Chem., Int. Ed.*, 2014, **53**, 1693–1698; (*c*) K.-R. Wang, D.-S. Guo, B.-P. Jiang and Y. Liu, *Chem. Commun.*, 2012, **48**, 3644–3646; (*d*) M. Gaeta, G. Sortino, R. Randazzo, I. Pisagatti, A. Notti, M. E. Fragalà, M. F. Parisi, A. D'Urso and R. Purrello, *Chem.–Eur. J.*, 2020, **26**, 3515–3518.

7 (*a*) L.-J. Chen, H.-B. Yang and M. Shionoya, *Chem. Soc. Rev.*, 2017, **46**, 2555–2576; (*b*) M. Pan, K. Wu, J.-H. Zhang and C.-Y. Su, *Coord. Chem. Rev.*, 2019, **378**, 333–349.

8 (*a*) Y. Domoto, M. Abe, T. Kikuchi and M. Fujita, *Angew. Chem., Int. Ed.*, 2020, **59**, 3450–3454; (*b*) Y. Domoto, M. Abe, K. Yamamoto, T. Kikuchi and M. Fujita, *Chem. Sci.*, 2020, **11**, 10457–10460; (*c*) Y. Domoto, M. Abe and M. Fujita, *J. Am. Chem. Soc.*, 2021, **143**, 8578–8582.

9 (*a*) M. M. Conn and J. Rebek, *Chem. Rev.*, 1997, **97**, 1647–1668; (*b*) D. L. Caulder and K. N. Raymond, *Acc. Chem. Res.*, 1999, **32**, 975–982; (*c*) R. W. Saalfrank, H. Maid and A. Schuerer, *Angew. Chem., Int. Ed.*, 2008, **47**, 8794–8824; (*d*) M. M. Smulders, I. A. Riddell, C. Brown and J. R. Nitschke, *Chem. Soc. Rev.*, 2013, **42**, 1728–1754; (*e*) T. R. Cook and J. P. Stang, *Chem. Rev.*, 2015, **115**, 7001–7045; (*f*) H. Hou, K. Zhou, F. Jiang, Q. Chen and M. Hong, *Isr. J. Chem.*, 2019, **59**, 140–150; (*g*) M. Han, D. M. Engelhard and G. H. Clever, *Chem. Soc. Rev.*, 2014, **43**, 1848–1860.

10 (*a*) H. Lang, A. Jakob and B. Milde, *Organometallics*, 2012, **31**, 7661–7693; (*b*) H. Schmidbaur and A. Schier, *Organometallics*, 2010, **29**, 2–23.

11 (*a*) M. O'Keeffe and M. M. J. Treacy, *Acta Cryst. A*, 2020, **76**, 611–621; (*b*) T. Castle, M. E. Evans and S. T. Hyde, *New J. Chem.*, 2008, **32**, 1484–1492; (*c*) S. T. Hyde and M. E. Evans, *Proc. Natl. Acad. Sci. U. S. A.*, 2022, **119**, e2110345118.

12 T. Sawada and M. Fujita, *Bull. Chem. Soc. Jpn.*, 2021, **94**, 2342–2350.

13 X. Zhao, H. Wang, B. Li, W. Zhang, X. Li, W. Zhao, C. Janiak, A. W. Heard, X.-J. Yang and B. Wu, *Angew. Chem., Int. Ed.*, 2022, **61**, e202115042.

14 (*a*) E. E. Fenlon, *Eur. J. Org. Chem.*, 2008, 5023–5035; (*b*) K. E. Horner, M. A. Miller, J. W. Steed and P. M. Sutcliffe, *Chem. Soc. Rev.*, 2016, **45**, 6432–6448; (*c*) S. D. P. Fielden, D. A. Leigh and S. L. Woltering, *Angew. Chem., Int. Ed.*, 2017, **56**, 11166–11194; (*d*) W.-X. Gao, H.-J. Feng, B.-B. Guo, Y. Lu and G.-X. Jin, *Chem. Rev.*, 2020, **120**, 6288–6325.

15 (*a*) N. Pairault and J. Niemeyer, *Synlett*, 2018, **29**, 689–698; (*b*) A. H. G. David and J. F. Stoddart, *Isr. J. Chem.*, 2021, **61**, 608–621; (*c*) J. R. J. Maynard and S. M. Goldup, *Chem*, 2020, **6**, 1914–1932; (*d*) Y. Sang and M. Liu, *Chem. Sci.*, 2022, **13**, 633–656.

16 J. Kobayashi, Y. Domoto and T. Kawashima, *Chem. Commun.*, 2009, 6186–6188.

17 Even the use of the ligand with longer side chain (**1d**) did not show the improvement of the diastereoselectivity (60 : 40) in the case of assembly **3**.

18 Significant solvent effects on diastereoselectivity were observed also for the self-assembly of the tetrahedral cages **3** (Fig. S8–S10†).

19 The sources and equivalents of the silver ($AgPF_6$ or $AgSbF_6$, 1.5–2.0 equiv.) and nitrate ions ($TMANO_3$ or $TBANO_3$, 0.5–1.5 equiv.) were adjusted to achieve complete convergence of the self-assembly process, which depends on the ligand used.

20 Treatment of the solution with a chiral-shift reagent anion (Δ-tris(tetrachlorobenzenediolate)phosphate(v) (Δ-TRISPHAT), 0–0.35 equiv., ref. 21) induced significant shifts of every ^{1}H NMR signal at 287 K (Fig. S14†), indirectly supporting the assignment as a pair of diastereomers.

21 (*a*) J. J. Jodry and J. Lacour, *Chem.–Eur. J.*, 2000, **6**, 4297–4304; (*b*) S. Hiraoka, K. Harano, T. Tanaka, M. Shiro and M. Shionoya, *Angew. Chem., Int. Ed.*, 2003, **42**, 5182–5185.